COMPRESSIBILITY EFFECTS IN A LARGE-EDDY SIMULATION OF A TURBULENT ROUND JET

Mohamed Maidi, Marcel Lesieur, Gwenaël Hauët
Laboratoire des Ecoulements Géophysiques et Industriels(LEGI),
BP 53, 38041 Grenoble Cedex 09,
FRANCE
Maidi@hmg.inpg.fr, Marcel.Lesieur@hmg.inpg.fr

ABSTRACT

This paper presents an application of large-eddy simulations (LES) to spatially-developing compressible round jets. Our goal is to demonstrate the ability of LES to reproduce and analyze the influence of the Mach number on the spatial development of compressible round jets. For Mach number $M = 0.9$ and Reynolds number 36000 the numerical simulation is shown to be in good agreement with DNS of Freund (1999) and experimental data of Stromberg et al. (1980). We show that at Mach 0.7 and for two different Reynolds number values ($Re = 2000, 36000$), the jet alternatively exhibits axisymmetric vortex structures (rings) and helical ones. Further downstream, they undergo alternate pairing as in the uniform-density case with the same upstream forcing. At $M = 1.4$ vortices are much more tilted in the flow direction, which is associated with an initail reduction of the jet spreading rate. Basic turbulent statistics and energy spectra are presented and assessed with respect to experiments.

INTRODUCTION

Due to their wide range of industrial applications in propulsion, combustion and acoustics, round jets have given rise to numerous analytical, experimental, and numerical studies. In a broad range of Reynolds numbers, jet dynamics is dominated by the presence of large coherent vortices up to twelve diameters from the nozzle. Experimental investigations of unforced jets have demonstrated the emergence of ring vortices in the transitional regime downstream of the nozzle (Michalke (1965), Becker and Massaro (1968), Crow and Champagne (1971), Zaman and Hussain (1980)). These vortices result from the development of Kelvin-Helmoltz (KH) instability. With proper forcings, Lasheras and Meiburg (1991) showed the emergence of streamwise hairpin vortices stretched between the KH rollers. Drubka (1981) observed visually other instability modes such as the helical mode in the potential-core region. Therefore, formation of these coherent vortices play a significant role in the jet spatial development and its spreading rate, but their nature depends strongly upon the inlet conditions existing in the experiments. The jets which will be simulated here are much different from real ones, since we just simulate the spatial development of a jet-like inflow profile perturbed by a weak random 3D white noise. The difference with reality may be particularly marked in the supersonic case, where the shock waves due to the nozzle cannot be simulated. LES techniques are a very good tool to investigate coherent-vortex dynamics in the transitional region of the jets at high Reynolds number. We have chosen here the *Structure Function* model originally proposed by Métais and Lesieur (1992) in its *Filtered* version (Ducros et al., 1996). Indeed, it removes the contribution of large-scale inhomogeneities to the eddy viscosity by the application to the velocity field of a Laplacien filter iterated three times.

NUMERICAL TECHNIQUE

We employ a finite-difference code utilizing a 4^{th} order Mac-Cormack scheme (1969) for spatial discretization and 2^{nd} order Gotlieb-Turkel scheme (1976) for time advancing. The computational Cartesian orthogonal grid has $100 \times 74 \times 74$ points in a box of 35, 16 and 16 nozzle radii respectively in the longitudinal and orthogonal directions. The grid is stretched, with accumulation of points close to the jet axis. Except for the inflow, boundary conditions are non-reflecting (Poinsot and Lele, 1992). To absorb outgoing acoustic disturbances and turbulent structures, there is downstream a sponge zone whose length is 20% of the computational domain length. The Mach number M is defined with the aid of the upstream jet center velocity U_0 and temperature, and the Reynolds number with U_0 and the upstream jet diameter D. First we validate our code by a comparisons with a DNS of Freund (1999) and the experiment of Stromberg et al (1980) at $M = 0.9$. Their Reynolds number is $Re = 3600$, and ours 36000, but it is well known that statistics of a turbulent round jet such as these shown in Figures 1 and 2 do not vary very much at lower Reynolds numbers ($Re \leq 50000$) (Zaman and Hussain, 1980). The upstream velocity profile is the same as Freund:

$$U = U_0[(0.5 - 0.5\tanh(2.8\left(\frac{r}{R} - \frac{R}{r}\right))(1 + \epsilon\sin(St.t))] \quad (1)$$

In which the Strouhal number $St = \frac{2Rf}{U}$ is 0.45 and the amplitude $\epsilon = 0.0025$. In Figure 1 we show the centerline velocity obtained from our LES model after a period of 900 D/U_0, compared with Freund's and Stromberg et al.'s data. Figure 2 shows the mean longitudinal velocity profiles for the same cases. The agreement is very good. For the following simulations, the inflow condition is as for the instability studies of Michalke and Hermann (1982):

$$U = \frac{U_1 + U_2}{2} + \frac{U_1 - U_2}{2}\tanh(\left(\frac{R}{\theta}\right)\left(\frac{r}{R} - \frac{R}{r}\right)) \quad (2)$$

Here U_1 is the jet centerline, U_2 is a small co-flow and θ the momentum thickness of the upstream shear layer. This mean velocity profile is perturbed by an isotropic 3D white noise. To visualize the jet structures, the Q-criterion isosurface technique is used (Hunt et al., 1988).

VORTEX DYNAMICS

Now we study the case $M = 0.7$ and two different Reynolds number values ($Re = 2000, 25000$). For both cases (see Figure 3 and 4), one sees upstream the shedding of axisymetric vortex rings. Further downstream, they undergo alternate pairing as the uniform density case (see Lesieur, 1997). At high Reynolds number the coherent vortices have a high amount of small-scale turbulence within them, which accelerates the transition mechanism towards a 3D turbulence which is not far from isotropy. This causes an increase of jet spreading rate (Figure 4).

We study now a higher Reynolds number of 36000. Figures 5 and 6 present two different times of evolution of the flow still at $M = 0.7$: Figure 5 (at $t = 30\ D/(U_1 - U_2)$) and Figure 6 (at $t = 300\ D/(U_1 - U_2)$). The flow field of Figure 5 corresponds to a transient stage close to initial computational time (at which the flow is periodic in the x-direction). It shows that the axisymmetric vortex rings persist up to $x/D = 6$. Between these vortex rings streamwise hairpin vortices are streched (see Figure 7). They have already been observed experimentally at moderate Reynolds number (Lasheras and Meiburg 1991, Liepmann and Gharib 1992). Further downstream, (at $x/D \approx 10$) they grow through an alternate pairing process (see Figure 5). This pairing mode corresponds to the growth of subharmonic perturbation developing after the formation of the primary vortex rings. Figure 6 does not present features basically different from Figure 4 . The instantaneous vorticity contours are shown in Figure 8 which also displays the transition from symmetric shear layer mode to asymmetric mode of vortex structures. Figure 9, at $M = 1.4$ and $t = 300\ D/(U_1 - U_2)$, corresponds to a statistically converged state. Compared with Figure 6, it shows that the vortices are much more tilted in the flow direction, associated with a reduction of the jet spreading width. This is in agreement with the plane mixing layer linear-stability results of Sandham and Reynolds (1989), and experimental findings of Papamoschou and Roshko (1988). The upstream axisymmetric mode has disappeared, but alternate pairing is still there. In fact, DNS of compressible plane temporal mixing layers presented in Lesieur (1997, pp: 119-125) show an inhibition of alternate pairing above a convective Mach number of $0.6 \approx 0.7$. Here, the convective Mach number is of the order of 0.7, and higher Mach number LES are needed in order to decide whether alternate pairing is cancelled by compressibility.

STATISTICAL RESULTS AND SPECTRAL ANALYSIS

The statistical evaluation is performed over the interval [$300\ D/(U_1 - U_2)$, $600\ D/(U_1 - U_2)$]. This corresponds to the time required for a vortex to cross the physical domain 20 times, and was sufficient to converge most turbulence statistics. We now take advantage of the apparent self-similar behavior and compare the LES at Mach 0.7 with incompressible jet measurement of Hussein et al. (1994) (Figure 10-a and 10-b). Overall, the agreement with experimental self-similar data is quite good. Nevertheless the normal streamwise Reynolds stresses (see Figure 10-a) are slightly over predicted for a radial distance smaller than $\eta = r/(x - x_0) < 0.06$, where x_0 is the virtual origin of the jet. Streamwise-radial cross stresses exhibit a very good agreement with the experimental data (Figure 10-b). Figure 11 shows the centerline streamwise velocity at Mach number 0.7 and Mach 1.4 respectively. The fall around $x/D = 6$ at Mach 0.7 indicates the end of the potential core where the shear layer thickness starts to develop inducing the increase of jet spreading rate, while at Mach 1.4 the end of the potential core is at about $x/D = 7$. Reynolds stresses ($< u'u' >$) are plotted in Figures 12 and 13. We show that the turbulence intensity increases with position x/D. In the vicinity of the potential core ($x/R = 14$ Figure 12, $x/R = 14.5$ Figure 13), it has reached its peak value in the middle of the shear layer around $r = R$. This peak at $r \approx R$ completely disappears at the final station plotted, which is expected as the jet changes from an initial annular shear layer form into a fully developed jet. It indeed appears that the jet has become fully developed by the right side of the physical portion of the computational domain ($x/R = 28$).

The downstream shear-layer growth in the subsonic and supersonic cases can be seen in Figure 14. Both cases of simulations yield similar results until $x/D \approx 6$. Beyond $x/D = 6$, the subsonic jet rapidly spreads, while the supersonic one spreads at a lower rate until $x/D \approx 10$. Further downstream the spreading rate of the supersonic jet ($M = 1.4$) increases to match that of the subsonic one.

It is important to check whether our simulated turbulence has a realistic broad-band energy spectrum. Figure 15 shows time spectra in the far field of the subsonic turbulent jet. The spectra are indeed broad-banded. There is a short $f^{-5/3}$ range. The presence of a short of dissipative range is certainly du to the close influence of the sponge zone.

Finally, Figures 16 and 17 show time spectra of the streamwise velocity signal at Mach 0.7 and Mach 1.4, taken on the centerline at the end of the potential core. At Mach 0.7 the peak is located at about $St = \frac{fD}{U(x=0,r=0)} = 0.39$ (Figure 16). While at Mach 1.4 the first frequency peak emerges around $St = 0.44$ (Figure 17). This is also well within experimental values ($0.3 \leq St \leq 0.5$, Hussain and Zaman, 1981). These values correspond to the preferred mode Strouhal number which indicates alternates pairing of large-scale vortices advected with the jet flow. Experiments of Crow and Champagne (1971) do show that the jet response is maximal in this range.

PERSPECTIVES

1) An extensive validation of the LES with experiment and DNS results at same inflow conditions which is currently under way.

2) Control of subsonic round jet at Mach 0.7, using the axial and flapping excitations at preferred and sub-harmonic frequencies, respectively.

SAMPLE REFERENCES

Becker, H. A., and Massaro, T. A., 1968, "Vortex evolution in a round jet", *J. Fluid Mech.*, vol. 31, pp. 435-448.

Crow, S. C., and Champagne, F. H., 1971, "Orderly structure in jet turbulence", *J. Fluid Mech.*, vol. 48, pp.547-591.

Da Silva, C. B., and Metais, O., 2002, "Vortex control of bifurcating jets: A numerical study", *Phys. Of Fuids.*, vol. 14, pp. 3798-3819.

Drubka, R. E., 1981, "Instabilities in near field of turbulent jets and their dependence on initial conditions and Reynolds number" *Ph.D. thesis, Departement of Mecanical and Aerospace Engineering, Illinois Institute of Technology.*

Ducros, F., Comte, P., and Lesieur, M., 1996, "Large-eddy simulation of transition to turbulence in a boundary layer developing spatially over a flat plate", *J. Fluid Mech.*, vol. 326, pp. 1-36.

Freund, J. B., 1999, "Acoustic sources in a turbulent jet: A direct numerical simulation study",*AIAA Paper*, 99-1858

Gottlieb, D. , and Turkel, E., 1976, "Dissipative two-four methods for time-dependent problems", *Math. Comp*, pp. 703-723.

Hunt, J. C. R., Wray, A. A., and Moin, P., 1988, "Eddies, stream and convergence zone in turbulent flows", *Annual Research Briefs*, (Center for Turbulence Research, Stanford University).

Hussein, H. J., Capp, S. P., and George, W. K., 1994, "Velocity measurements in high-Reynolds number, momentum-conserving, axisymmetric, turbulent jet", *J. Fluid Mech.*, vol. 258, pp. 31-75.

Hussain, F., and Zaman, K. B. M. Q., 1981, "The preferred mode of the axisymmetric jet", *J. Fluid Mech.*, vol. 110, pp. 39-71.

Lasheras, J. C., and Meiburg, E., 1991, " On the three-dimensional dynamics of coherent vortical structures forming in free, shear flow", in *Turbulence and coherent structures*, O. Métais and M. Lesieur eds, *Kluwer Academic Publisher*, pp. 91-111.

Lesieur, M., and Métais, O., 1999, "New trends in large-eddy simulations of turbulence", *Annu. Rev. Fluid Mech.*, vol. 28, pp. 45-98.

Lesieur, M., 1997, "Turbulence in Fluids: third ed.", *Kluwer Academic Publisher.*

Liepmann, D., and Gharib, M., 1992, "The role of the streamwise vorticity in the near-field entrainement of round jets", *J. Fluid Mech.*, vol. 245, pp. 643-688.

Mac Cormack, R. W., 1969, "The effects of viscosity in hypervelocity impact cratering", *AIAA Paper*, 169-354.

Métais, O., and Lesieur, M., 1992, "Spectral large eddy simulation of isotropic and stably stratified turbulence", *J. Fluid Mech.*, vol. 239, pp. 157-194.

Michalke, A., 1965, "On spatially growing disturbances in an inviscid shear layer", *J. Fluid Mech.*, vol. 23, pp. 521-544.

Michalke, A., and Hermann, G., 1982, "On the inviscid instability of a circular jet with external flow", *J. Fluid Mech.*, vol. 114, pp. 343-359.

Papamoschou, D., and Roshko, A., 1988, "The compressible turbulent shear layer: an experimental study", *J. Fluid Mech.*, vol. 197, pp. 453-477.

Poinsot, T. J., and Lele, S. K., 1992, "Boundary conditions for direct simulations of compressible viscous flows",*J. Comput. Phys*, vol. 101, pp. 104-129.

Sandham, N. D., and Reynolds, W. C., 1989, "The compressible mixing layer: linear theory and direct simulation", *AIAA Paper*, 89-0371.

Stromberg, J. L., Mclaughlin, D. K., and Troutt, T. R., 1980, "Flow field and acoustic properties of a Mach number 0.9 jet at low Reynolds number",*J. of Sound & Vib*, vol. 72, pp. 159-176.

Zaman, K. B. M. Q., and Hussain, A. K. M. F., 1980, " Vortex pairing in a circular jet under controlled excitation, part1, general jet response", *J. Fluid Mech.*, vol. 101, pp. 449-491.

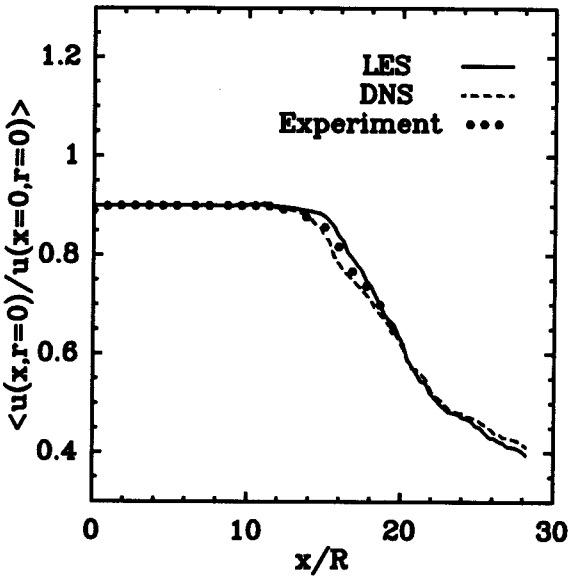

Figure 1: Mean centerline velocity obtained at Mach 0.9 from the LES, DNS (Freund 1999), and experiment (Stromberg et al., 1980).

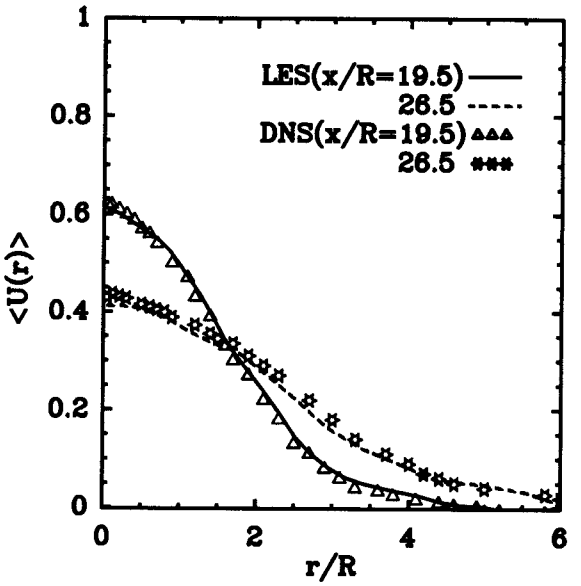

Figure 2: Same calculation as Fig. 1. Mean velocity at various different downstream positions.

Figure 3: Isosurfaces of Q criterion for the natural jet at $Re = 2000$, $M = 0.7$ and $t = 300D/(U_1 - U_2)$.

Figure 4: Isosurfaces of Q criterion for the natural jet at $Re = 25000$, $M = 0.7$ and $t = 300D/(U_1 - U_2)$.

Figure 5: Spatial evolution of coherent vortices shown by isosurface of positive Q for the natural jet at $Re = 36000$, $M = 0.7$ and $t = 30D/(U_1 - U_2)$.

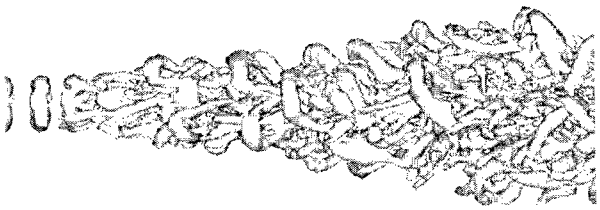

Figure 6: Isosurfaces of Q criterion for the natural jet at $Re = 36000$, $M = 0.7$ and $t = 300D/(U_1 - U_2)$.

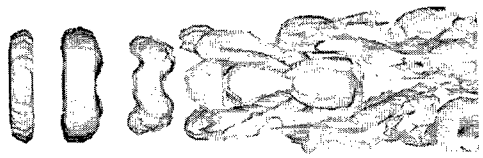

Figure 7: Visualization of the streamwise hairpin vortex by isosurfaces of Q criterion for the natural jet at $Re = 36000$, $M = 0.7$ and $t = 100D/(U_1 - U_2)$.

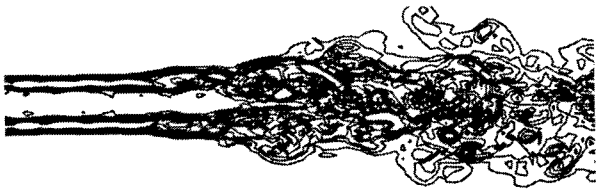

Figure 8: Vorticity magnitude cross section for the natural jet at $Re = 36000$, $M = 0.7$ and $t = 300D/(U_1 - U_2)$.

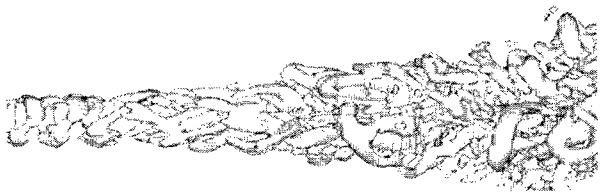

Figure 9: Isosurfaces of Q criterion for the natural jet at $Re = 36000$, $M = 1.4$ and $t = 300D/(U_1 - U_2)$.

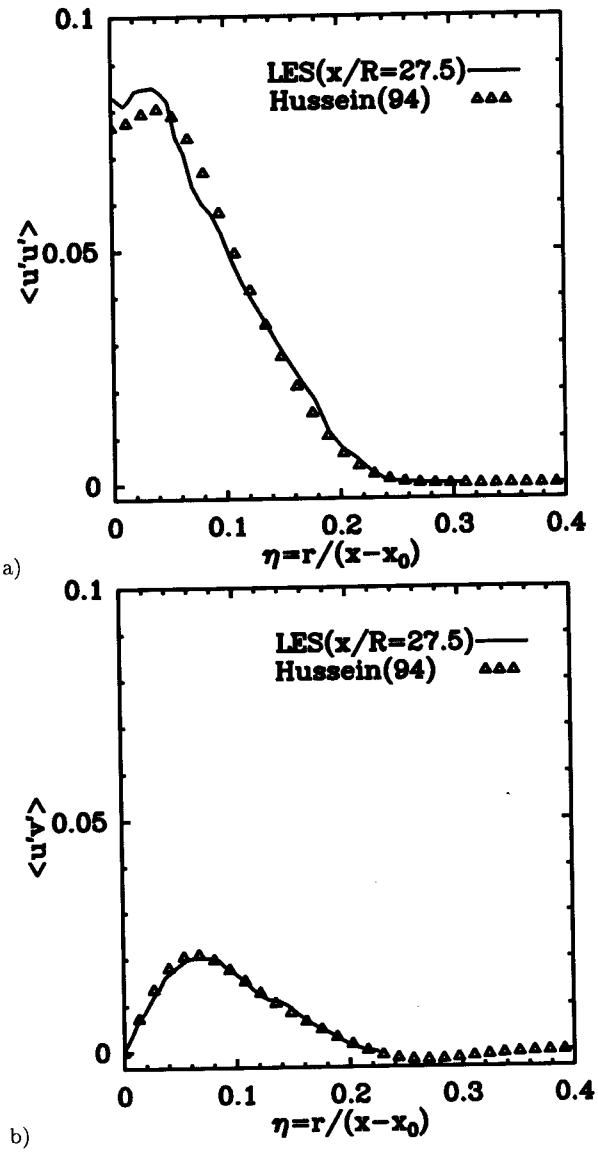

Figure 10: Reynolds shear stress profiles at the far field for the natural jet at $M = 0.7$: a) streamwise normal stresses, b) streamwise and radial cross stresses.

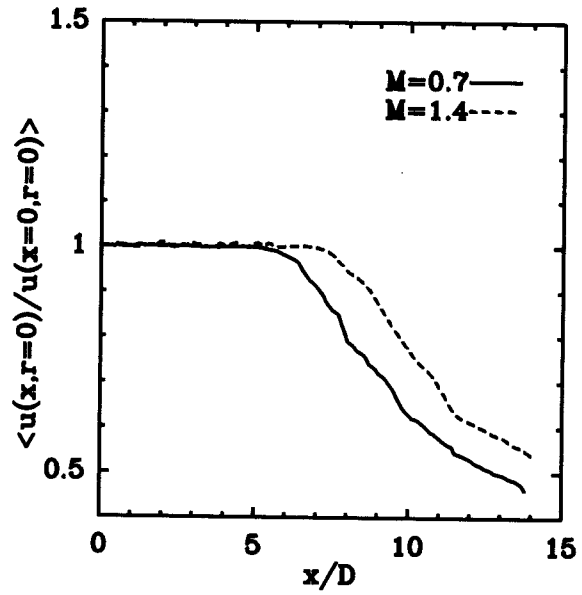

Figure 11: Mean centerline velocity as a function of the longitudinal coordinate x/D, for the natural jet at $M = 0.7$ and $M = 1.4$.

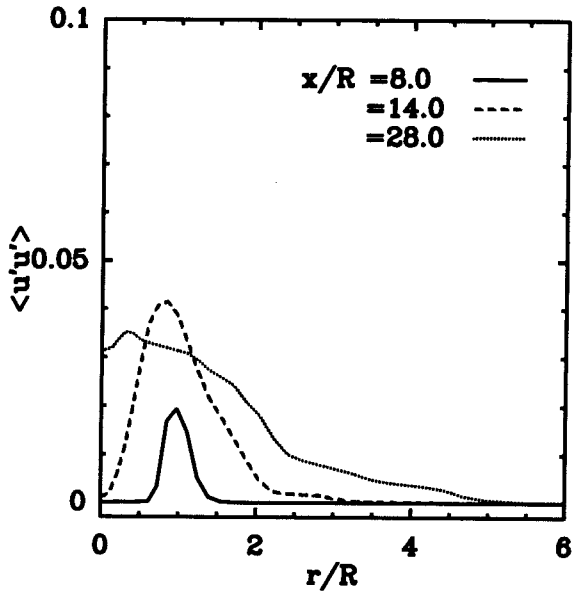

Figure 13: Axial Reynolds shear stress profiles at various different downstream positions for the natural jet at $M = 1.4$.

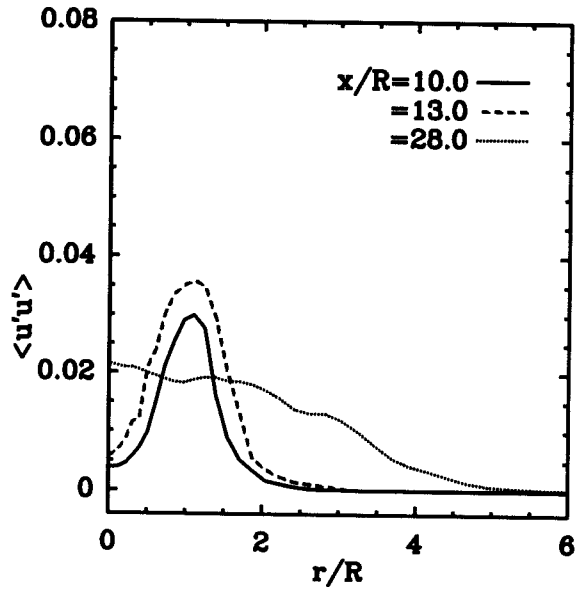

Figure 12: Axial Reynolds shear stress profiles at various different downstream positions for the natural jet at $M = 0.7$.

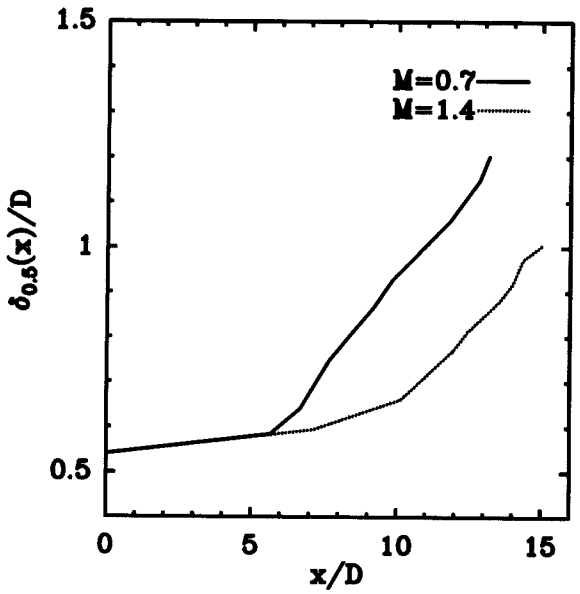

Figure 14: Streamwise evolution of the shear layer thickness.

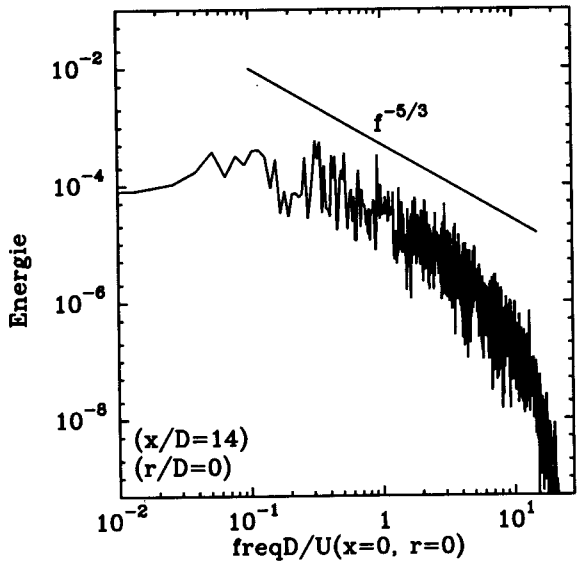

Figure 15: Temporal spectra of the streamwise velocity at far field region for the natural jet at $M = 0.7$ and $Re = 36000$.

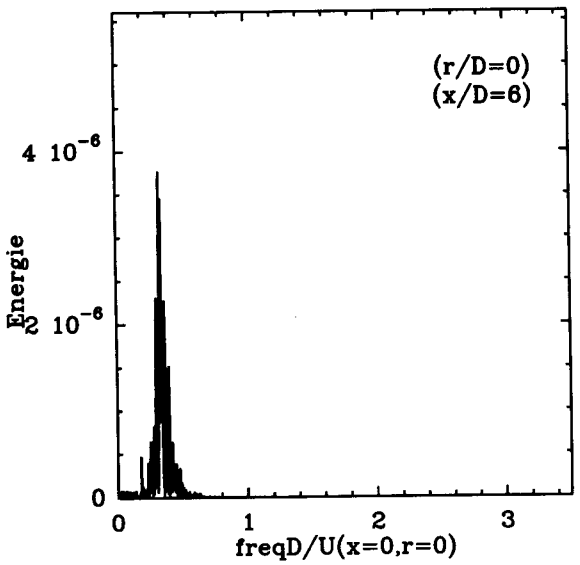

Figure 16: Temporal spectra of the streamwise velocity for the natural jet at $M = 0.7$.

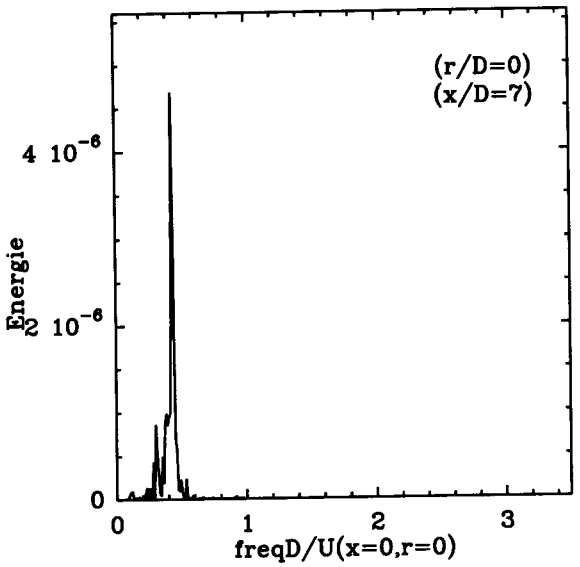

Figure 17: Temporal spectra of the streamwise velocity for the natural jet at $M = 1.4$.